Inorganic Chemistry
Article

Inorg. Chem. **2009**, *48*, 6731–6739 **6731**
DOI: 10.1021/ic9006789

One-Dimensional Ce^{3+}- and/or Tb^{3+}-Doped X_1-Y_2SiO_5 Nanofibers and Microbelts: Electrospinning Preparation and Luminescent Properties

Lili Wang, Zhiyao Hou, Zewei Quan, Chunxia Li, Jun Yang, Hongzhou Lian, Piaoping Yang, and Jun Lin*

State Key Laboratory of Rare Earth Resource Utilization, Changchun Institute of Applied Chemistry, Chinese Academy of Sciences, Changchun 130022, P. R. China, and Graduate University of the Chinese Academy of Sciences, Beijing 100049, P. R. China

Received April 7, 2009

One-dimensional X_1-Y_2SiO_5:Ce^{3+} and -Tb^{3+} nanofibers and quasi-one-dimensional X_1-Y_2SiO_5:Ce^{3+} and -Tb^{3+} microbelts have been prepared by a simple and cost-effective electrospinning process. X-ray powder diffraction, Fourier transform infrared spectroscopy, scanning electron microscopy (SEM), energy-dispersive X-ray spectrometry, transmission electron microscopy, high-resolution transmission electron microscopy, photoluminescence (PL), and cathodoluminescence spectra were used to characterize the samples. SEM results indicate that the as-prepared fibers and belts are smooth and uniform with a length of several tens to hundreds of micrometers, whose diameters decrease after being annealed at 1000 °C for 3 h. Under ultraviolet excitation and low-voltage electron beam excitation, the doped rare earth ions show their characteristic emission, that is, Ce^{3+} 5d−4f and Tb^{3+} $^5D_4$−^7F_J (J = 6, 5, 4, 3) transitions, respectively. PL excitation and emission spectra demonstrated that there is an energy transfer from Ce^{3+} to Tb^{3+} in the X_1-Y_2SiO_5:Ce^{3+},Tb^{3+} samples. Additionally, the X_1-Y_2SiO_5:Ce^{3+} and -Tb^{3+} microbelt phosphors show a higher emission intensity than that of nanofiber phosphors under UV and low-voltage electron beam excitation.

1. Introduction

One-dimensional (1D) nanostructural materials, such as nanofibers, nanowires, and nanorods, have attracted great research interest because of their potential in fundamental studies and technological applications.[1−3] Quasi-one-dimensional (Q-1D) nanostructural materials also have attracted intensive experimental and theoretical interest as a result of their novel physical properties and potential applications.[4] As one subgroup of Q-1D structural materials, microbelts still remain significant due to promising properties.[5] Up to now, there have been many methods reported for the synthesis of 1D and Q-1D nanomaterials with different compositions, including chemical or physical vapor deposition,[6] solution,[7] laser ablation,[8] arc discharge,[9] a vapor-phase transport process,[10] and a template-based method.[11] In comparison to these methods, electrospinning is a more simple, convenient, cost-effective, and versatile technique for generating long fibers with diameters ranging from tens of nanometers up to micrometers. The electrospinning method was first developed in the 1930s,[12] and now it has been demonstrated that a variety of materials can be electrospun to form uniform fibers, such as organic, inorganic, and hybrid polymers (organic−inorganic composites).[13] The fibers prepared by electrospinning have good orientation, a large specific surface area, a large aspect ratio, and dimensional stability, which can be applied in sensors, electronic and optical devices, biomedical fields, and catalyst supports.[14]

*To whom correspondence should be addressed. E-mail: jlin@ciac.jl.cn.

(1) Lauhon, L. J.; Gudiksen, M. S.; Wang, D.; Lieber, C. M. *Nature* **2002**, *420*, 57.
(2) Wu, Y. Y.; Yan, H. Q.; Huang, M.; Messer, B.; Song, J. H.; Yang, P. D. *Chem.—Eur. J.* **2002**, *8*, 1260.
(3) Hu, J.; Ouyang, M. Y.; Lieber, C. M. *Nature* **1999**, *399*, 48.
(4) (a) Alivisator, A. P. *Science* **1996**, *271*, 933. (b) Hu, J.; Odom, T. W.; Lieber, C. M. *Acc. Chem. Res.* **1999**, *32*, 435. (c) Wong, E. W.; Sheehan, P. E.; Lieber, C. M. *Science* **1997**, *277*, 1971.
(5) Zhao, Y.; Zhu, X.; Huang, Y. Y.; Wang, S. X.; Yang, J. L.; Xie, Y. *J. Phys. Chem. C* **2007**, *111*, 12145.
(6) (a) Fu, L.; Liu, Y. Q.; Hu, P.; Xiao, K.; Yu, G.; Zhu, D. B. *Chem. Mater.* **2003**, *15*, 4287. (b) Bae, S. Y.; Seo, H. W.; Park, J.; Yang, H.; Park, J. C.; Lee, S. Y. *Appl. Phys. Lett.* **2002**, *81*, 126.
(7) Trentler, T. J.; Hickman, K. M.; Goel, S. C.; Viano, A. M.; Gibbons, P. C.; Buhro, W. E. *Science* **1995**, *270*, 1791.
(8) Duan, X. F.; Lieber, C. M. *Adv. Mater.* **2000**, *12*, 298.
(9) Jung, J. H.; Kobayashi, H.; Van Bommel, K. J. L.; Shinkai, S.; Shimizu, T. *Chem. Mater.* **2002**, *14*, 1445.
(10) (a) Wu, Y.; Yang, P. *Chem. Mater.* **2000**, *12*, 605. (b) Chen, C. C.; Yeh, C. C. *Adv. Mater.* **2000**, *12*, 738.
(11) Teo, W. E.; Ramakrishna, S. *Nanotechnology* **2006**, *17*, R89.
(12) Formhals, A. U.S. Patent Specification, **1934**, 1975504.
(13) (a) Li, D.; Xia, Y. *Nano. Lett.* **2003**, *3*, 555. (b) Ding, B.; Kim, H.; Kim, C.; Khil, M.; Park, S. *Nanotechnology* **2003**, *14*, 532. (c) Li, D.; Ouyang, G.; Xia, Y. *Nano Lett.* **2005**, *5*, 913. (d) Madhugiri, S.; Dalton, A.; Gutierrez, J.; Ferraris, J. P.; Balkus, K. J.Jr. *J. Am. Chem. Soc.* **2003**, *125*, 14531.
(14) (a) Wang, X. Y.; Drew, C.; Lee, S. H.; Senecal, K. J.; Kumar, J.; Samuelson, L. A. *Nano Lett.* **2002**, *2*, 1273. (b) Liu, H. Q.; Kameoka, J.; Czaplewski, D. A.; Craighead, H. G. *Nano Lett.* **2004**, *4*, 671. (c) Czaplewski, D. A.; Kameoka, J.; Mathers, R.; Coates, G. W.; Craighead, H. G. *Appl. Phys. Lett.* **2003**, *83*, 4836. (d) Casper, C. L.; Stephens, J. S.; Tassi, N. G.; Chase, D. B.; Rabolt, J. F. *Macromolecules* **2004**, *37*, 573.

Published on Web 06/12/2009

Table 1. Summary of the Experiment Conditions and the Corresponding Morphologies

sample	volume ratio of water and ethanol (v/v)	type of PVP/wt % of PVP	voltage (kV)/distance (cm)/spinning rate (mL/h)	morphology
Y_2SiO_5: 5 mol % Tb^{3+} Y_2SiO_5: 3 mol % Ce^{3+} Y_2SiO_5: 5 mol % Tb^{3+}, 3 mol % Ce^{3+}	1/2	K-30, SCRC/36.5 wt %	15/16/1	nanofibers
Y_2SiO_5: 5 mol % Tb^{3+} Y_2SiO_5: 3 mol % Ce^{3+} Y_2SiO_5: x% Tb^{3+}, 3 mol % Ce^{3+} (x=1, 2, 3, 4, 5)	2/3	M_w=1,300,000, Aldrich/8 wt %	9/17/1	microbelts

Rare earth oxyorthosilicates RE_2SiO_5 (RE = rare earths) have been studied for a long time because of their efficient luminescence under UV, cathode-ray, and X-ray excitation. There are two structures: the monoclinic X_1 type for species containing larger RE^{3+} (La−Tb) with the $P2_1/c$ space group and the X_2 type for smaller RE^{3+} (Dy−Sc) in the $B2/b$ space group. For Y_2SiO_5, the low-temperature modification belongs to the X_1 type, whereas the high-temperature form belongs to the X_2 type.[15] It is well-known that Y_2SiO_5 is an ideal host material for both photoluminescent (PL) and cathodoluminescent (CL) phosphors. Ce^{3+} and Tb^{3+} ions are two important RE ions, which have been applied in blue and green phosphors. Yttrium silicates doped with Ce^{3+} and Tb^{3+} ions are well-known phosphor materials used in fluorescent lamps, cathode ray tubes, and field emission displays due to their highly saturated color and strong luminescence.[15b] So, quite a few papers have been published on the luminescence properties of rare-earth-ion-doped X_1-Y_2SiO_5 in the powder,[15c] thin film,[15a] core/shell-structure,[15b] or single crystal forms,[16] and there are also many methods reported for the synthesis of Ce^{3+}- and Tb^{3+}-doped Y_2SiO_5 phosphors, including sol−gel process,[15b] spray pyrolysis method,[17] pulsed laser deposition,[18] and soft lithography.[15a] In general, compared with bulk materials, the shape of the 1D structure provided a better model system to investigate the dependence of electronic transport and optical properties on size confinement and dimensionality.

As far as we know, the synthesis of 1D and Q-1D Ce^{3+}- and Tb^{3+}-doped X_1-Y_2SiO_5 phosphor materials via the electrospinning process has not been reported. Accordingly, in this article, we report the preparation of 1D fiberlike and Q-1D beltlike Ce^{3+}- and Tb^{3+}-doped X_1-Y_2SiO_5 phosphors via a simple and cost-effective electrospinning method. Moreover, we also investigate the structure, morphology, and PL and CL properties of the resulting samples in detail.

2. Experimental Section

Materials. The main starting materials were Y_2O_3, Tb_4O_7, $Ce(NO_3)_3\cdot 6H_2O$ (all with a purity of 99.99%, Science and Technology Parent Company of Changchun Institute of Applied Chemistry, China), tetraethyl orthosilicate $Si(OC_2H_5)_4$ (TEOS, 99 wt %, analytical reagent, A. R., Beijing Yili Fine Chemical Co., Ltd.), poly(vinylpyrrolidone) (PVP; M_w = 1 300 000, Aldrich; PVP, K-30, Sinopharm Chemical Reagent Co., Ltd.; the two kinds of PVPs have different molecular weights, which will further influence the morphology of the products), and nitric acid, HNO_3. All of the materials were used without further purification. Ethanol C_2H_5OH (A. R.) and deionized water were used as solvents.

Preparation. Nanofibers of X_1-Y_2SiO_5:Tb^{3+} and/or -Ce^{3+} phosphors were prepared by an electrospinning process. The doping concentrations of Tb^{3+} ions are 1−5 mol % of Y^{3+} in X_1-Y_2SiO_5, while the Ce^{3+} ions are fixed at 3 mol %.[15b] Stoichiometric amounts of Y_2O_3, Tb_4O_7, and $Ce(NO_3)_3\cdot 6H_2O$ (1.25 mmol) were dissolved in dilute HNO_3 with vigorous stirring and heating. Then, 12 mL of a water−ethanol solution (v/v = 1:2) as well as a stoichiometric amount of TEOS (0.28 mL) were added to the above solution under magnetic stirring for 1 h, resulting in the formation of a transparent solution. Finally, a certain amount of poly(vinylpyrrolidone) (PVP, K-30, Sinopharm Chemical Reagent Co., Ltd.) was added to adjust the viscoelastic behavior of the solution (the weight percentage of PVP is 36.5% in the water−ethanol solution). The solution was stirred for 8 h to obtain a homogeneous hybrid solution for further electrospinning. The above viscous solution was placed in a 10 mL hypodermic syringe. The anode of the high-voltage power supply was clamped to the syringe needle tip, and the cathode was connected to the grounded collector plate. The applied voltage was 15 kV, and the distance between the needle tip and the collector was 16 cm. The flow rate of the spinning solution was controlled at 1 mL/h by a syringe pump (TJ-3A/W0109−1B, Boading Longer Precision Pump Co., Ltd., China). The electrospun products were then calcined at 1000 °C for 3 h with a heating rate of 2 °C/min. In a typical process for the preparation of X_1-Y_2SiO_5:Tb^{3+} and/or -Ce^{3+} microbelts, the solution for electrospinning was prepared using a similar procedure by changing the ratio of the water−ethanol solution together with the type and amount of PVP. Typically, the ratio of the water−ethanol solution was adjusted to 2:3 by volume; another kind of poly(vinylpyrrolidone) (PVP, M_w = 1 300 000, Aldrich) was added with a weight percentage of 8% in the water−ethanol solution. The solution was also stirred for 8 h to obtain a homogeneous viscous solution for electrospinning. The distance between the needle tip and the collector was changed to 17 cm, and the applied voltage was tuned to 9 kV. The flowing rate was also controlled at 1 mL/h by the syringe pump. The as-prepared precursor products were then annealed at 1000 °C with a heating rate of 2 °C/min and held there for 3 h in the air. In this way, X_1-Y_2SiO_5:Tb^{3+} and/or -Ce^{3+} nanofibers and microbelts were prepared, respectively. The detailed experimental parameters (optimized ones) for obtaining these two different morphologies are summarized in Table 1.

Characterization. The X-ray powder diffraction (XRD) measurements were carried out on a Rigaku-Dmax 2500 diffractometer using Cu Kα radiation (λ = 0.15405 nm). FT-IR spectra were measured with Perking-Elmer 580B infrared

(15) (a) Han, X. M.; Lin, J.; Fu, J.; Xing, R. B.; Yu, M.; Zhou, Y. H.; Pang, M. L. *Solid State Sci.* **2004**, *6*, 349. (b) Lin, C. K.; Wang, H.; Kong, D. Y.; Yu, M.; Liu, X. M.; Wang, Z. L.; Lin, J. *Eur. J. Inorg. Chem.* **2006**, 3667. (c) Lin, J.; Su, Q.; Zhang, H. J.; Wang, S. B. *Mater. Res. Bull.* **1996**, *31*, 189. (d) Reichardt, J.; Stiebler, M.; Hirrle, R.; Kermmler-Sack, S. *Phys. Status Solidi A* **1990**, *119*, 631. (e) Ito, J.; Johnson, H. *Am. Mineral.* **1968**, *53*, 1940.

(16) (a) Lin, J.; Su, Q.; Wang, S. B.; Zhang, H. J. *J. Mater. Chem.* **1996**, *6*, 265. (b) Shin, S. H.; Jeon, D. Y.; Suh, K. S. *Jpn. J. Appl. Phys.* **2001**, *L40*, 4715.

(17) Kang, Y. C.; Lenggoro, I. W.; Okuyama, K.; Park, S. B. *J. Electrochem. Soc.* **1999**, *146*, 1227.

(18) Gonzalez-Ortega, J. A.; Perea, N.; Hirata, G. A. *Opt. Mater.* **2006**, *29*, 47.

spectrophotometer with the KBr pellet technique. The morphology and composition of the samples were inspected using a field emission scanning electron microscope (FESEM; XL30, Philips) equipped with an energy-dispersive X-ray spectrometer (EDS; JEOL JXA-840). Transmission electron microscopy (TEM) and high-resolution transmission electron microscopy (HRTEM) micrographs were obtained from a FEI Tecnai G2 S-Twin transmission electron microscope with a field emission gun operating at 200 kV. An inductively coupled plasma optical emission spectrometer (ICP-OES; ICAP 6300, Thermal Scientific) was used to determine the actual doping concentration of Tb^{3+} ions in X_1-Y_2SiO_5 nanofibers. The photoluminescence (PL) measurements were performed on a Hitachi F-4500 spectrophotometer equipped with a 150 W xenon lamp as the excitation source. The CL measurements were carried out in an ultrahigh-vacuum chamber ($< 10^{-8}$ Torr), where the samples were excited by an electron beam at a voltage range of 1−3 kV with different filament currents, and the emission spectra were recorded using an F-4500 spectrophotometer. All of the measurements were performed at room temperature.

3. Results and Discussion

Formation and Morphology. XRD. Figure 1 shows the XRD patterns of the Y_2SiO_5:Tb^{3+} (5 mol % Tb^{3+}) (a), Y_2SiO_5:Ce^{3+} (3 mol % Ce^{3+}) (b), and Y_2SiO_5:Tb^{3+}, Ce^{3+} (5/3 mol % Tb^{3+}/Ce^{3+}) (c) nanofibers annealed at 1000 °C for 3 h, as well as the standard card of X_1-Y_2SiO_5 (JCPDS no. 52-1810) as a reference. For the Ce^{3+}- and Tb^{3+}-doped Y_2SiO_5 nanofibers calcined at 1000 °C, a crystalline X_1-Y_2SiO_5 phase can be seen (Figure 1), and all of the diffraction peaks can be assigned exactly to the standard card of X_1-Y_2SiO_5 (JCPDS no. 52-1810). No second phase is detected at this doping level, indicating that the Ce^{3+} and Tb^{3+} ions can be efficiently built into the X_1-Y_2SiO_5 host lattice by substitution for the Y^{3+} ion. The XRD results of Ce^{3+}- and Tb^{3+}-doped Y_2SiO_5 microbelts demonstrate that their crystallization behaviors are similar to those of the nanofibers and will not be shown here anymore.

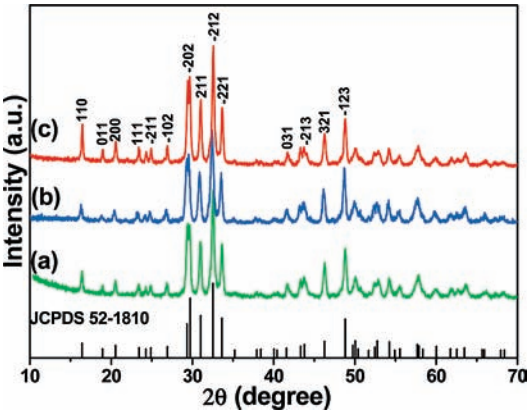

Figure 1. X-ray diffraction patterns of Y_2SiO_5:Tb^{3+} (5 mol % Tb^{3+}) (a), Y_2SiO_5:Ce^{3+} (3 mol % Ce^{3+}) (b), and Y_2SiO_5:Tb^{3+},Ce^{3+} (5/3 mol % Tb^{3+}/Ce^{3+}) (c) nanofibers annealed at 1000 °C for 3 h as well as the standard card of X_1-Y_2SiO_5 (JCPDS no. 52-1810) as a reference.

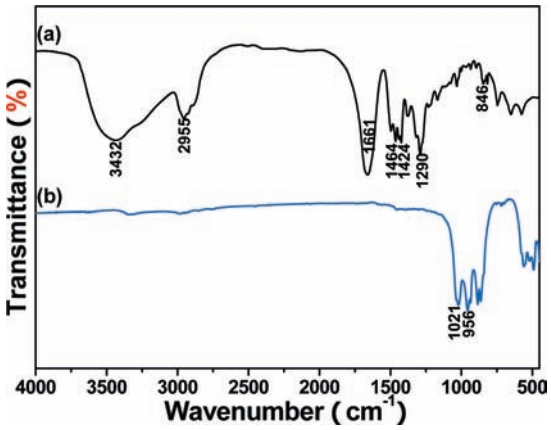

Figure 2. FT-IR spectra of as-prepared precursor for Y_2SiO_5:Tb^{3+} (5 mol % Tb^{3+}) fibers (a) and those calcined at 1000 °C (b).

FT-IR. The FT-IR spectra of the as-prepared precursor for Y_2SiO_5:Tb^{3+} (5 mol % Tb^{3+}) nanofibers and those annealed at 1000 °C are shown in parts a and b of Figure 2, respectively. The broad band at 3432 cm^{-1} is assigned to the symmetric stretching vibration of −OH groups, which can be clearly observed from Figure 2a. The IR spectrum of the as-prepared precursor sample also shows the characteristic stretching band corresponding to the amide carbonyl group (1661 cm^{-1}), which is probably superimposed by the water bending vibrations (∼1660 cm^{-1}); $-CH_2$ group (2955, 1464, and 1424 cm^{-1}); and tertiary amide group (1290 cm^{-1}), which arise from the starting materials (ethanol and PVP).[19,20] These bands cannot be observed in the Y_2SiO_5:Tb^{3+} (5%) fibers which annealed at 1000 °C for 3 h (Figure 2b). The other obvious band at 846 cm^{-1} in Figure 2a can be ascribed to the symmetric stretching vibration of Si−O−Si.[21,22] After heating at 1000 °C, the absorption peaks from the organic components disappear completely, and the new bands peaking at 1021 and 956 cm^{-1} in Figure 2b are present, which may arise from the asymmetric and symmetric stretching vibration of Si−O−Si, respectively.[23,15a]

SEM and TEM. The morphologies and structures of samples were investigated by SEM and TEM observations. The SEM images and EDS of as-formed nanofibers are shown in Figure 3. The low-magnification SEM images of as-prepared Y_2SiO_5:Tb^{3+} (5 mol % Tb^{3+}) nanofibers (Figure 3A) and those annealed at 1000 °C (Figure 3C) indicated that the fibers are uniform with a length of several tens to hundreds of micrometers. It can be seen that the as-prepared precursor fibers are smooth and uniform with diameters ranging from 200 to 450 nm (Figure 3A,B). In order to obtain pure inorganic fibers, a high annealing temperature is employed to remove the organic PVP templates. After being annealed at high temperatures, the fiber diameters decrease greatly, accompanied by the changes on the surface properties (inset of Figure 3D) due to the decomposition of the organic species and the formation of inorganic phase. The diameters of the nanofibers (seem to consist of linked particles) calcined at 1000 °C for 3 h become 70−140 nm

(19) Williames, D. H.; Fleming, I. *Spectroscopic Methods in Organic Chemistry*; McGraw-Hill Book Company Limited: London, 1987; p 40.
(20) Zhao, Y. Y.; Wang, H. Y.; Lu, X. F.; Li, X.; Yang, Y.; Wang, C. *Mater. Lett.* **2008**, *62*, 143.
(21) (a) Kook Mah, S.; Chung, I. J. *J. Non-Cryst. Solids* **1995**, *183*, 252. (b) Kioul, A.; Mascia, L. *J. Non-Cryst. Solids* **1994**, *175*, 169.
(22) Chen, Y.; Iron, J. O. *Chem. Mater.* **1999**, *11*, 1218.
(23) Lin, J.; Sänger, D. U.; Mennig, M.; Bärner, K. *Thin Solid Films* **2000**, *360*, 39.

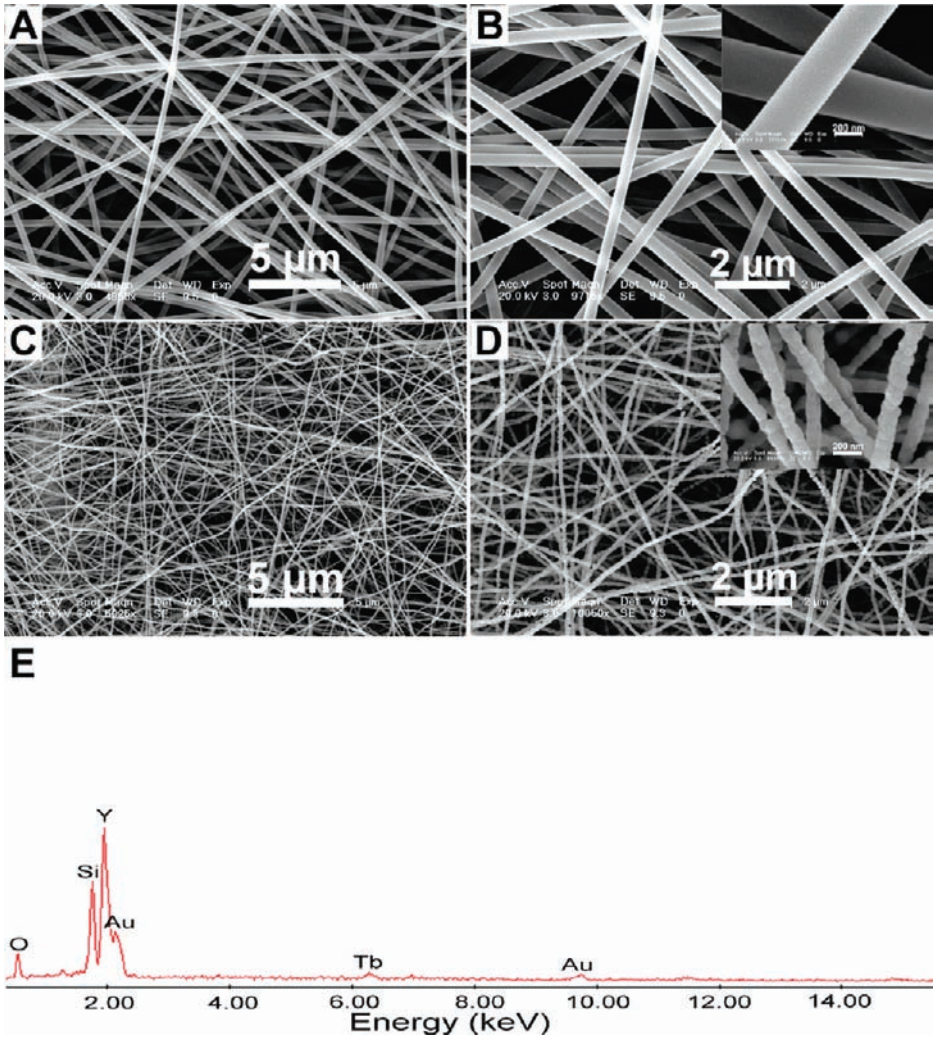

Figure 3. SEM images for the as-formed precursor for Y_2SiO_5:Tb^{3+} (5 mol % Tb^{3+}) nanofibers—images with low magnification (A) and high magnification (B)—and those annealed at 1000 °C—images with low magnification (C), high magnification (D), and EDS pattern (E).

(Figure 3C, D). The EDS was used to characterize the composition of the fibers annealed at 1000 °C, as in Figure 3E. The presence of O, Si, Y, and Tb in Figure 3E further indicates the formation of Y_2SiO_5 (containing Tb) in the fibers. The presence of a Au peak arises from the coated Au layer on the sample in the course of SEM measurement. The actual doping molar concentration of Tb^{3+} ions in X_1-Y_2SiO_5 nanofibers was determined by ICP optical emission spectrometery, and it is shown that the actual doping concentration of Tb^{3+} is about 5.2 mol % of Y^{3+} in X_1-Y_2SiO_5 nanofibers, basically agreeing with the nominal result (5 mol %).

Figure 4 shows the typical TEM (A) and the HRTEM images of the X_1-Y_2SiO_5:Tb^{3+} (5 mol % Tb^{3+}) nanofibers annealed at 1000 °C. In Figure 4A, fibers with a diameter of 102 nm can be observed clearly, which is well-consistent with that observed from the SEM images (Figure 3C,D). From the HRTEM image of X_1-Y_2SiO_5:Tb^{3+} (5 mol % Tb^{3+}) nanofibers (Figure 4B), we can see crystalline phase (X_1-Y_2SiO_5) with well-resolved lattice fringes. The distance (0.2760 nm) between the adjacent lattice fringes just corresponds to the interplanar distance of Y_2SiO_5 (−212) planes, agreeing well with the d (−212) spacing of the literature value (0.2750 nm; JCPDS no. 52-1810). These results further confirm the formation of crystalline X_1-Y_2SiO_5 in the fibers, agreeing well with the XRD results.

The fibers with a variety of cross-sectional shapes can be prepared by the electrospinning method.[24] Usually, the electrospun fibers have a cylindrical cross section. The morphology and diameters of the fibers can be influenced by many electrospinning parameters; these parameters include the type of polymer, the conformation of the polymer chain, the viscosity of the solution, the solution conductivity, and the operational conditions. However, under control of these factors, the beltlike morphology phosphors will be obtained, which might be a result of the formation of a skin on the surface of the liquid jet (due to rapid evaporation of solvent) and the subsequent collapse of the skin.[25] Additionally, incomplete fiber drying before reaching the grounded collector will lead to the formation

(24) (a) Ra, E. J.; An, K. H.; Kim, K. K.; Jeong, S. Y.; Lee, Y. H. *Chem. Phys. Lett*. **2005**, *413*, 188. (b) Song, T.; Zhang, Y. Z.; Zhou, T. J.; Lim, C. T.; Ramakrishna, S.; Liu, B. *Chem. Phys. Lett*. **2005**, *415*, 317. (c) Viswanathamurthi, P.; Bhattarai, N.; Kim, H. Y.; Lee, D. R.; Kim, S. R.; Morris, M. A. *Chem. Phys. Lett*. **2003**, *374*, 79.

(25) (a) Li, D.; Xia, Y. N. *Adv. Mater*. **2004**, *16*, 1151. (b) Zhang, Y. F.; Yang, J.; Li, Q.; Cao, X. Q. *J. Cryst. Growth* **2007**, *308*, 180.

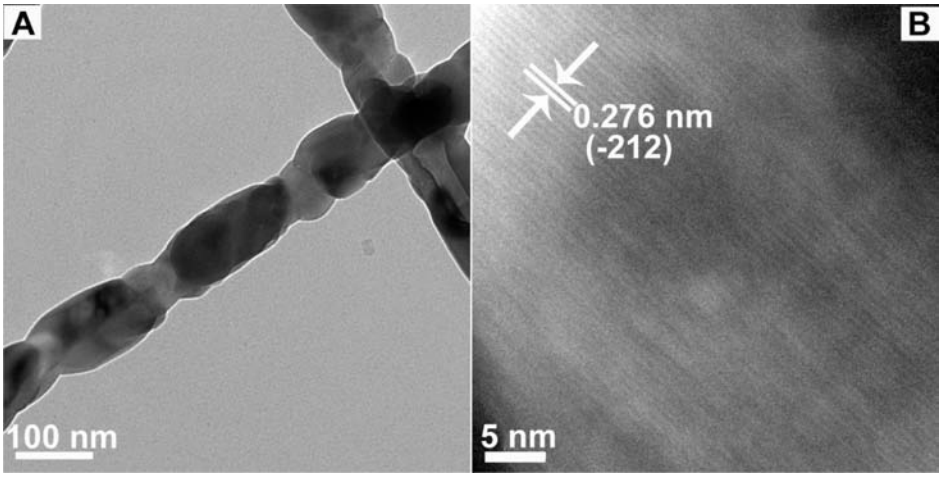

Figure 4. TEM (A) and HRTEM (B) images of Y_2SiO_5:Tb^{3+} (5 mol % Tb^{3+}) nanofibers annealed at 1000 °C.

of beltlike structures with rectangular cross sections.[26] By changing the experimental conditions as shown in Table 1, the beltlike structure of X_1-Y_2SiO_5: Tb^{3+} and/or -Ce^{3+} phosphors can also be obtained by the electrospinning process. Figure 5 presents the low and high SEM images of the as-prepared precursor for Y_2SiO_5:Tb^{3+} (5 mol % Tb^{3+}) microbelts and those annealed at 1000 °C. It can be seen that the as-formed precursor belts are smooth and uniform with an average width of 0.84 μm and a thickness of 0.37 μm (Figure 5A,B). After being annealed at 1000 °C for 3 h, the sample maintains a beltlike structure with an average width of 0.62 μm and a thickness of 0.20 μm (Figure 5C,D).

Finally, it should be mentioned that the key factor in the electrospinning method to obtain 1D inorganic nanomaterials was to form a solution with a suitable viscoelastic behavior similar to that of a conventional polymer solution. In order to obtain uniform 1D morphologies, it is very important to search for a balance point of various electrospinning parameters. In our experiments, the balance point might be related to the volume ratio of water to ethanol, the strength of applied voltage, the weight percentage of PVP, and the distance between the needle tip and the collector. The synthesis conditions listed in Table 1 are the optimized ones for the corresponding morphologies.

Luminescence Properties. Photoluminescence Properties of Y_2SiO_5:Tb^{3+} Nanofibers and Microbelts. Y_2SiO_5:Tb^{3+} samples (with different morphologies) exhibit a strong green emission under UV irradiation. Figure 6 shows the excitation (a) and emission (b) spectra of the Y_2SiO_5:Tb^{3+} (5 mol % Tb^{3+}) nanofibers (black lines) and microbelts (green lines). It can be seen clearly that the excitation and emission spectra of the two samples are similar in shape, and the bands differ only in their intensities. The excitation spectrum (Figure 6a) contains an intense broad band with a maximum at 248 nm corresponding to the spin-allowed $4f^8-4f^75d$ transition ($\Delta S = 0$) of Tb^{3+}, and a weak broad band at 287 nm due to the spin-forbidden component of the $4f^8-4f^75d$ transition ($\Delta S = 1$). The energy difference between these two transitions is 5479 cm^{-1}, agreeing well with the theoretical value (6000 cm^{-1}) reported previously.[15a,27] Also, the excitation lines in the longer-wavelength region within the Tb^{3+} $4f^8$ electron configuration cannot be seen in this magnification due to their weak intensity. Excitation into the spin-allowed $4f^8-4f^75d$ band at 248 nm yields the characteristic emission lines of Tb^{3+} $^5D_4-^7F_J$ (J = 3, 4, 5, 6) transitions, with the $^5D_4-^7F_5$ (542 nm) green emission as the most prominent group (Figure 6b). Under identical measurement conditions, the relative intensities of two samples are different; namely, the microbelt phosphors have a higher PL intensity than that of the nanofiber phosphors. It is well-known that the surface area of materials increases along with a decrease in size. The large surface area introduces a large number of defects into the phosphor crystal. Defects have a serious drawback in PL intensity for phosphors, as they provide nonradiative recombination routes for electrons and holes.[28] Herein, the surface areas of the as-prepared Y_2SiO_5:Tb^{3+} (5 mol % Tb^{3+}) microbelts are much smaller than those of Y_2SiO_5:Tb^{3+} (5 mol % Tb^{3+}) nanofibers because the former is much bigger than the latter in size (Figures 3D and 4D). This is the reason that the PL intensity of microbelts is higher than that of nanofibers.

Photoluminescence Properties of Y_2SiO_5:Ce^{3+} Nanofibers and Microbelts. Y_2SiO_5:Ce^{3+} samples (with different morphologies) exhibit a strong blue emission under UV irradiation. The excitation (a) and emission (b) spectra of the Y_2SiO_5:Ce^{3+} (3 mol % Ce^{3+}) nanofibers (black lines) and microbelts (blue lines) are shown in Figure 7. It can be seen clearly that the excitation spectrum (monitored at 437 nm) consists of a strong band with a maximum at 367 nm and a weak band at 282 nm, corresponding to the transitions from the ground state $^2F_{5/2}$ to the excited 5d states of Ce^{3+}. The emission spectrum (monitored at 367 nm) of Ce^{3+} consists of a broad band with a maximum at 437 nm, which is ascribed to the parity-allowed

(26) Sill, T. J.; von Recum, H. A. *Biomaterials* **2008**, *29*, 1989.

(27) (a) Blasse, G.; Bril, A. *Philips Res. Repts.* **1967**, *22*, 481. (b) Lin, J.; Su, Q. *J. Mater. Chem.* **1995**, *5*, 1151.

(28) (a) Wan, J. X.; Wang, Z. H.; Chen, X. Y.; Mu, L.; Qian, Y. T. *J. Cryst. Growth* **2005**, *284*, 538. (b) Yang, J.; Liu, X. M.; Li, C. X.; Quan, Z. W.; Kong, D. Y.; Lin, J. *J. Cryst. Growth* **2007**, *303*, 480. (c) Yang, J.; Li, C. X.; Cheng, Z. Y.; Zhang, X. M.; Quan, Z. W.; Zhang, C. M.; Lin, J. *J.Phys. Chem. C* **2007**, *111*, 18148.

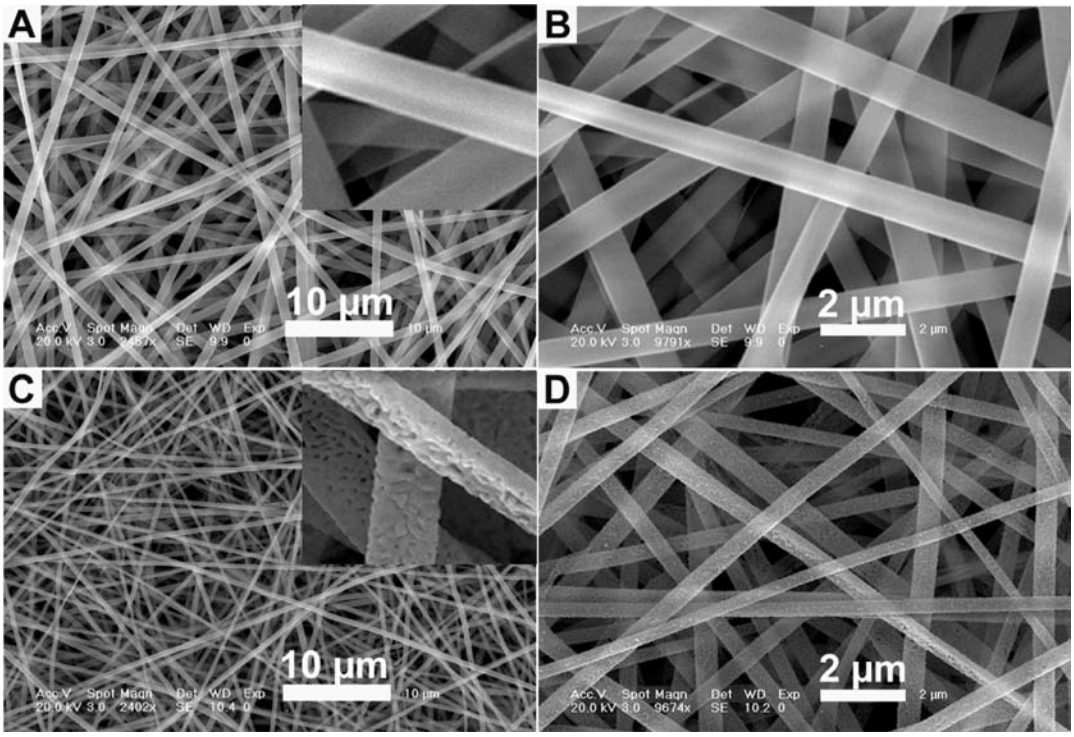

Figure 5. SEM images for the as-formed precursor for $Y_2SiO_5:Tb^{3+}$ (5 mol % Tb^{3+}) microbelts—images with low magnification (A) and high magnification (B)—and those annealed at 1000 °C—images with low magnification (C) and high magnification (D).

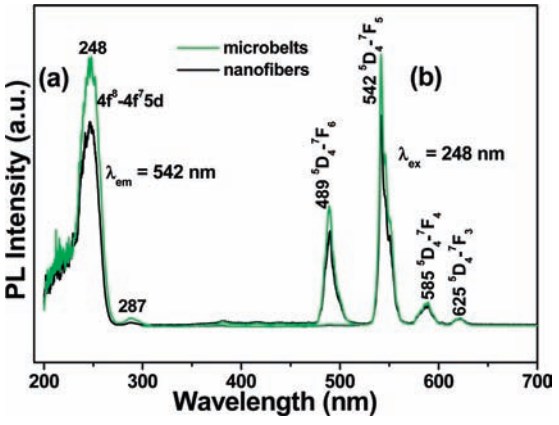

Figure 6. Excitation (a) and emission (b) spectra of the X_1-$Y_2SiO_5:Tb^{3+}$ (5 mol % Tb^{3+}) nanofibers (black lines) and microbelts (green lines).

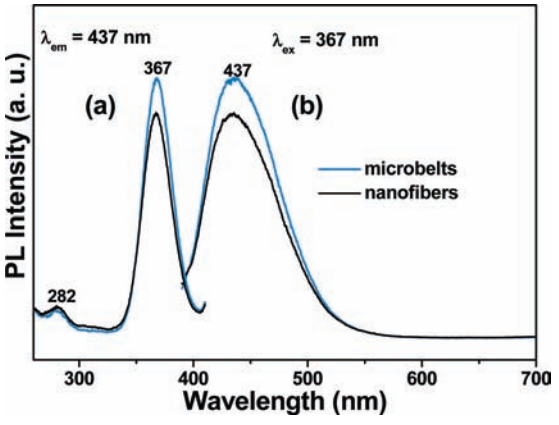

Figure 7. Excitation (a) and emission (b) spectra of the X_1-$Y_2SiO_5:Ce^{3+}$ (3 mol % Ce^{3+}) nanofibers (black lines) and microbelts (blue lines).

transitions of the lowest component of the 5d state to the ground state of Ce^{3+}.[15] The $Y_2SiO_5:Ce^{3+}$ microbelts also have a higher PL intensity than that of the nanofibers due to the same reason as given above.

Photoluminescence Properties of $Y_2SiO_5:Ce^{3+}$, Tb^{3+} Nanofibers and Microbelts. Figure 8 presents the excitation (a) and emission (b) spectra of the $Y_2SiO_5:Tb^{3+}$, Ce^{3+} (5/3 mol % Tb^{3+}, Ce^{3+}) nanofibers (black lines) and microbelts (green lines). The excitation spectrum, monitored with the 542 nm emission ($^5D_4-^7F_5$) of Tb^{3+} is composed of a strong band at 248 nm, a weak band at 282 nm, and an intense band at 367 nm (Figure 8a). In comparison with the excitation spectra of $Y_2SiO_5:Tb^{3+}$ (5 mol % Tb^{3+}) (Figure 6a) and $Y_2SiO_5:Ce^{3+}$ (3 mol % Ce^{3+}) (Figure 7a), the first band is ascribed to the $4f^8-4f^7$5d transitions of Tb^{3+}, and the latter two bands originate from the 4f−5d transitions of Ce^{3+}, which indicates that energy transfer has occurred from Ce^{3+} to Tb^{3+} in the $Y_2SiO_5:Tb^{3+},Ce^{3+}$ (5/3 mol % Tb^{3+}, Ce^{3+}) samples (with different morphologies). Excitation into the Ce^{3+} excitation band at 367 nm yields both the emission of Ce^{3+} (390−470 nm) and that of Tb^{3+} ($^5D_4-^7F_J$ at 489, 542, 585, 625 nm), which is further indicative of the energy transfer from Ce^{3+} to Tb^{3+} in $Y_2SiO_5:Tb^{3+}$, Ce^{3+} (5/3 mol % Tb^{3+}, Ce^{3+}) samples. Additionally, it can be clearly seen that the $Y_2SiO_5:Tb^{3+},Ce^{3+}$ (5/3 mol % Tb^{3+}, Ce^{3+}) microbelts also have a higher PL intensity than that of nanofibers, and the reasons have been stated in the photoluminescence sections for $Y_2SiO_5:Tb^{3+}$ (5 mol % Tb^{3+}).

In order to investigate the energy-transfer process from Ce^{3+} to Tb^{3+} in $Y_2SiO_5:Ce^{3+},Tb^{3+}$ microbelt samples in

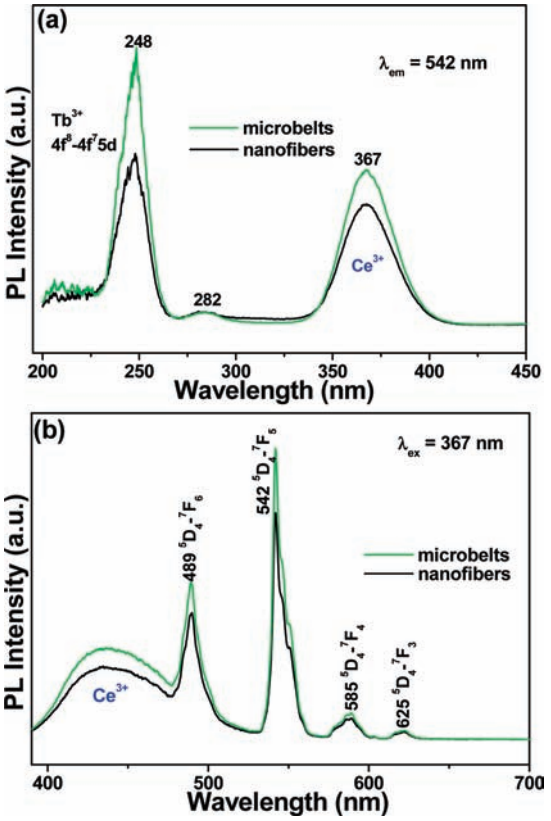

Figure 8. Excitation (a) and emission (b) spectra of the X_1-Y_2SiO_5:Tb^{3+},Ce^{3+} (5/3 mol % Tb^{3+},Ce^{3+}) nanofibers (black lines) and microbelts (green lines).

more detail, a series of emission spectra (excited at 367 nm) of Y_2SiO_5:Ce^{3+}, $x$$Tb^{3+}$ microbelts (keeping Ce^{3+} ions fixed at 3 mol %) with different concentrations of Tb^{3+} ions are shown in Figure 9. In Figure 9a, the characteristic emission of Ce^{3+} ions is present exclusively when the doping concentration of Tb^{3+} is zero, $x = 0\%$. For other samples, it can be seen that both characteristic emission from Ce^{3+} in the blue spectral region and prominent emission from Tb^{3+} in the green spectral region can be detected under an excitation of 367 nm. Moreover, the PL intensity of Tb^{3+} ions (monitored at 367 nm) increases with the increasing doping Tb^{3+} concentrations from 1% to 5 mol % in Y_2SiO_5:Ce^{3+}, $x$$Tb^{3+}$ microbelts (3% Ce^{3+}). Therefore, it is obvious that, under an excitation of 367 nm, the Ce^{3+} ions become excited, and the energy absorbed can be released by itself to yield the blue emission or can be transferred to Tb^{3+} ions and then released by Tb^{3+} ions to give the characteristic emission lines ($^5D_4-{}^7F_J$, $J = 3, 4, 5, 6$), with the $^5D_4-{}^7F_5$ (542 nm) green emission as the prominent group. Figure 9b presents the corresponding CIE chromaticity coordinates positions. The CIE chromaticity coordinates change from $x = 0.1472$, $y = 0.0703$ (blue) to $x = 0.1914$, $y = 0.2693$ (bluish-green) by varying the doping concentration of Tb^{3+} ions from $x = 0$ to $x = 5$ mol % in Y_2SiO_5:Ce^{3+}, $x$$Tb^{3+}$ (3 mol % Ce^{3+}) samples. The corresponding luminescence color can change from blue to bluish-green.

Figure 10 shows a summary of the emission and energy-transfer processes in Y_2SiO_5:Tb^{3+}, Ce^{3+} (5/3 mol % Tb^{3+}, Ce^{3+}) samples. Under UV light excitation, an electron on the Ce^{3+} ion is excited from the ground state

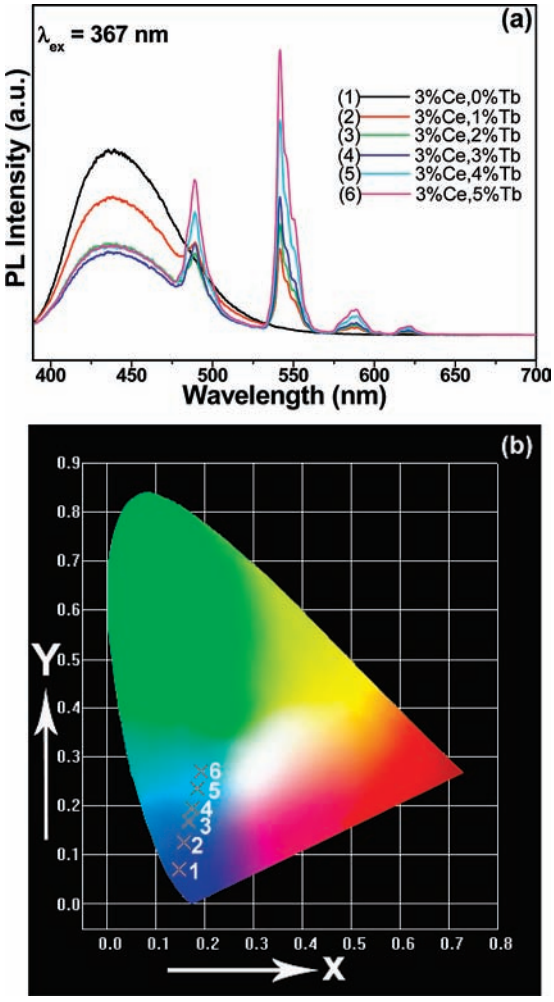

Figure 9. Photoluminescence spectra of X_1-Y_2SiO_5:Ce^{3+} (3 mol % Ce^{3+}), $x$$Tb^{3+}$ microbelts with different Tb^{3+} ion concentrations (x = 0, 1, 2, 3, 4, 5 mol %; $\lambda_{ex} = 367$ nm) (a) and the corresponding CIE chromaticity diagram (b).

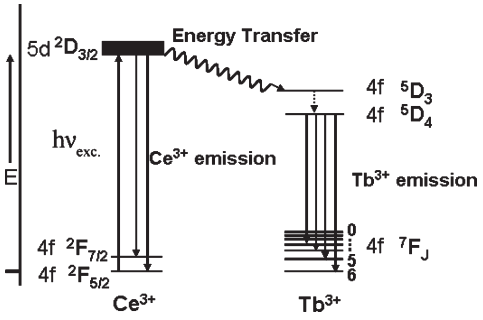

Figure 10. Scheme of energy transfer from Ce^{3+} to Tb^{3+}.

(4f) to the excited state (5d). In the excited state, this electron either relaxes to the lowest 5d crystal-field-splitting state then returns to the ground state to produce the blue emission or transfers its excitation energy to the higher excited energy levels of Tb^{3+} ($4f^8$), which relax to the $^5D_4$ level, where the green emission ($^5D_4-{}^7F_J$) takes place.[15b,29] Competition between the above two processes

(29) (a) Jose, M. T.; Lakshmanan, A. R. *Opt. Mater.* **2004**, *24*, 651. (b) Bourcet, J.-C.; Fong, F. K. *J. Chem. Phys.* **1974**, *60*, 34. (c) Wang, Z. L.; Quan, Z. W.; Lin, J.; Fang, J. *J. Nanosci. Nanotech.* **2005**, *5*, 1532.

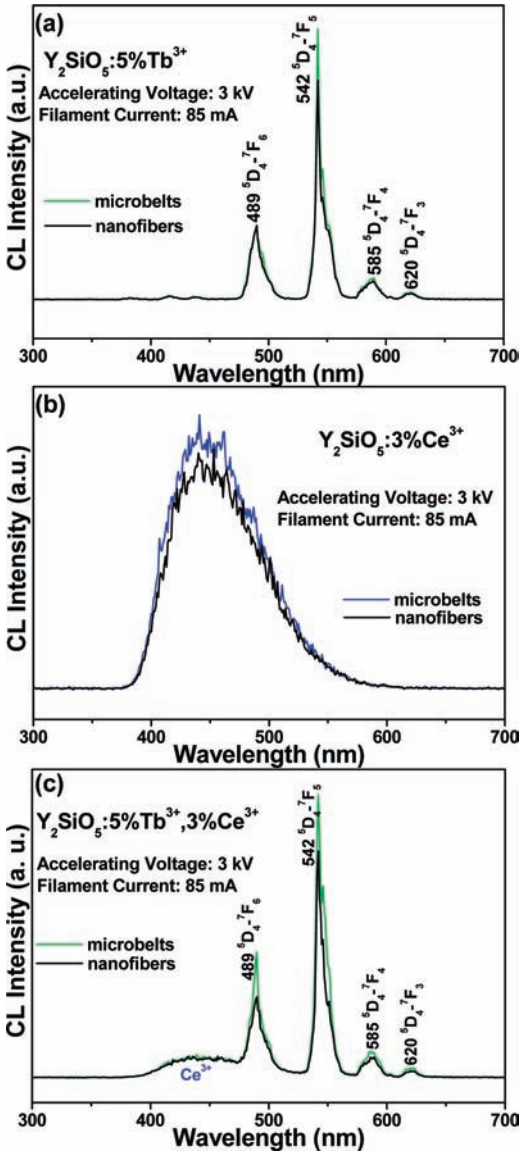

Figure 11. Typical cathodoluminescence spectra of X_1-Y_2SiO_5:Tb^{3+} (5 mol % Tb^{3+}) (a); X_1-Y_2SiO_5:Ce^{3+} (3 mol % Ce^{3+}) (b); and X_1-Y_2SiO_5:Tb^{3+}, Ce^{3+} (5/3 mol % Tb^{3+}, Ce^{3+}) (c) microbelts and nanofibers. (Accelerating voltage = 3 kV; filament current = 85 mA.)

results in the occurrence of emission from Ce^{3+} and Tb^{3+} simultaneously in Y_2SiO_5:Tb^{3+}, Ce^{3+} (5/3 mol % Tb^{3+}, Ce^{3+}) samples (Figure 8b).

Cathodoluminescence Properties of Ce^{3+}- and/or Tb^{3+}-Doped Y_2SiO_5 Nanofibers and Microbelts. Under the low-voltage electron beam excitation, the as-prepared Y_2SiO_5:Tb^{3+} (5 mol % Tb^{3+}), Y_2SiO_5:Ce^{3+} (3 mol % Ce^{3+}), and Y_2SiO_5:Tb^{3+}, Ce^{3+} (5/3 mol % Tb^{3+}, Ce^{3+}) nanofibers and microbelts also exhibit strong green, blue, and blue-green luminescence, respectively. Typical CL spectra of the samples under the excitation of an electron beam (accelerating voltage = 3 kV; filament current = 85 mA) are shown in Figure 11, which have shapes identical to the PL emission spectra. Similarly, from the typical CL spectra, it can be seen that the microbelt phosphors have a higher CL intensity than that of nanofiber phosphors (all of the experimental conditions were kept identical in order to avoid experimental errors), which can also be explained by the same reason given above. The CL

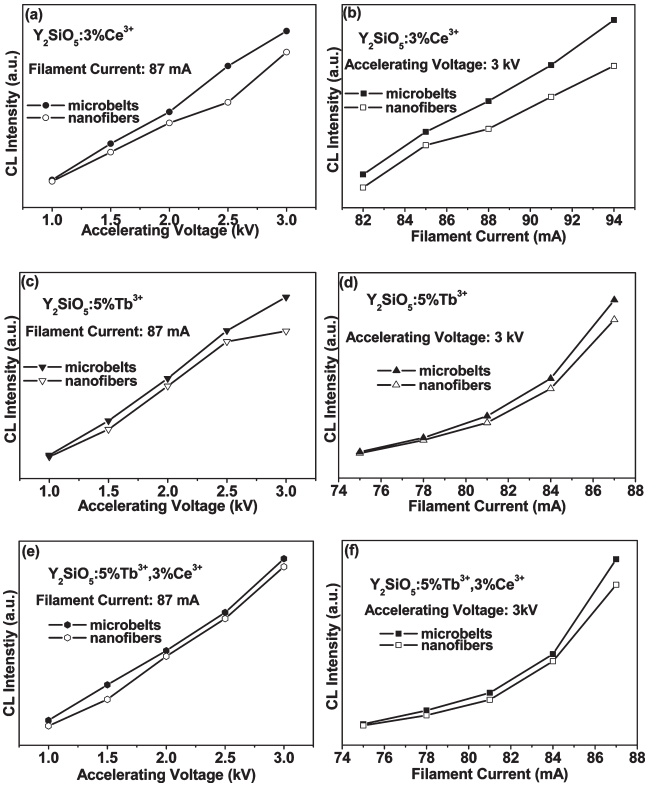

Figure 12. Cathodoluminescence intensity of Ce^{3+}- and/or Tb^{3+}-doped X_1-Y_2SiO_5 microbelts and nanofibers as a function of accelerating voltage (a, c, e) and filament current (b, d, f).

emission intensities for Y_2SiO_5:Tb^{3+} (5 mol % Tb^{3+}), Y_2SiO_5:Ce^{3+} (3 mol % Ce^{3+}), and Y_2SiO_5:Tb^{3+}, Ce^{3+} (5/3 mol % Tb^{3+}, Ce^{3+}) nanofibers and microbelts have been investigated as a function of the accelerating voltage and the filament current, as shown in Figure 12. When the filament is fixed at 87 mA, the CL intensities of Y_2SiO_5:Ce^{3+} (3 mol % Ce^{3+}), Y_2SiO_5:Tb^{3+} (5 mol % Tb^{3+}), and Y_2SiO_5:Tb^{3+}, Ce^{3+} (5/3 mol % Tb^{3+}, Ce^{3+}) nanofibers and microbelts increase upon raising the acceleration voltage from 1 to 3 kV (Figure 12a,c,e). Similarly, under a 3 kV electron beam excitation, the CL intensity of Y_2SiO_5:Ce^{3+} (3 mol % Ce^{3+}) nanofibers and microbelts also increases with an increase of the filament current from 82 to 94 mA (Figure 12b), and the CL intensity of Y_2SiO_5:Tb^{3+} (5 mol % Tb^{3+}) and Y_2SiO_5:Tb^{3+}, Ce^{3+} (5/3 mol % Tb^{3+}, Ce^{3+}) nanofibers and microbelts increases with an increase of the filament current from 75 to 87 mA (Figure 12d,f). The increase in CL brightness with an increase in electron energy and filament current are attributed to deeper penetration of the electron into the phosphor's body and the larger electron beam current density. The electron penetration depth can be estimated by the empirical formula L50 [Å] = 250 $(A/\rho)(E/Z^{1/2})^n$, where $n = 1.2/(1 - 0.29 \log_{10} Z)$, where A is the atomic or molecular weight of the material, ρ is the bulk density, Z is the atomic number or the number of electrons per molecule in the case compounds, and E is the accelerating voltage (kV).[30] For cathodoluminescence, the Ce^{3+} and Tb^{3+} ions are excited by the plasma produced by the incident electrons. The deeper the electron penetration

(30) Feldman, C. *Phys. Rev.* **1960**, *117*, 455.

depth, the more the plasmons will be produced, which results in more Ce^{3+} and Tb^{3+} ions being excited, and thus the CL intensity increases.

4. Conclusions

In summary, Ce^{3+}- and/or Tb^{3+}-doped X_1-Y_2SiO_5 one-dimensional nanofibers and quasi-one-dimensional microbelts have been successfully prepared by a simple and versatile electrospinning method. The as-formed precursor samples present a smooth surface and uniform fiberlike and beltlike morphologies with a length of several tens to hundreds of micrometers. After being heated at 1000 °C for 3 h, the as-formed samples are well-crystallized and still maintain their original morphologies, except for the decreasing diameters. Under UV and low-voltage electron beam excitation, the samples show blue and green luminescence, respectively, and the microbelt phosphors have a higher emission intensity than that of nanofiber phosphors. These studies indicate a facile route for the development of 1D and Q-1D luminescent nanomaterials that are useful in many types of color display fields.

Acknowledgment. This project is financially supported by National Basic Research Program of China (2007CB935502) and the National Natural Science Foundation of China (NSFC 50702057, 50872131, 00610227).